

# On the electronically nonadiabatic decomposition dynamics of furazan and triazole energetic molecules

Cite as: J. Chem. Phys. **150**, 164304 (2019); <https://doi.org/10.1063/1.5088995>

Submitted: 16 January 2019 . Accepted: 02 April 2019 . Published Online: 24 April 2019

Jayanta Ghosh , Harshad Gajapathy , Ajay Jayachandran, Elliot R. Bernstein, and Atanu Bhattacharya 



View Online



Export Citation



CrossMark

## ARTICLES YOU MAY BE INTERESTED IN

[Performance of trajectory surface hopping method in the treatment of ultrafast intersystem crossing dynamics](#)

The Journal of Chemical Physics **150**, 164126 (2019); <https://doi.org/10.1063/1.5079426>

[Calculation of the absolute photoionization cross-sections for C1-C4 Criegee intermediates and vinyl hydroperoxides](#)

The Journal of Chemical Physics **150**, 164305 (2019); <https://doi.org/10.1063/1.5088408>

[Franck-Condon factors by counting perfect matchings of graphs with loops](#)

The Journal of Chemical Physics **150**, 164113 (2019); <https://doi.org/10.1063/1.5086387>

The Journal  
of Chemical Physics

2018 EDITORS' CHOICE

READ NOW!



# On the electronically nonadiabatic decomposition dynamics of furazan and triazole energetic molecules

Cite as: J. Chem. Phys. 150, 164304 (2019); doi: 10.1063/1.5088995

Submitted: 16 January 2019 • Accepted: 2 April 2019 •

Published Online: 24 April 2019



View Online



Export Citation



CrossMark

Jayanta Ghosh,<sup>1</sup> Harshad Gajapathy,<sup>1</sup> Ajay Jayachandran,<sup>1</sup> Elliot R. Bernstein,<sup>2</sup>  
and Atanu Bhattacharya<sup>1,a)</sup>

## AFFILIATIONS

<sup>1</sup>Department of Inorganic and Physical Chemistry, Indian Institute of Science, Bangalore 560012, India

<sup>2</sup>Department of Chemistry, Colorado State University, Fort Collins, Colorado 80523, USA

<sup>a)</sup>atanub@iisc.ac.in and atanubhattach@gmail.com

## ABSTRACT

The combined results of *ab initio* electronic-structure calculations, nonadiabatic molecular dynamics simulations using *ab initio* multiple spawning, and previous spectroscopic investigations of jet-cooled molecules provide strong evidence of a  $(\pi, \sigma^*)$ -mediated decomposition mechanism for the furazan and triazole energetic molecules. The importance of dissociative excited states formed by electron promotion from a  $\pi$  molecular orbital to a  $\sigma^*$  molecular orbital is explored for the furazan and triazole energetic molecules. Dissociative  $(\pi, \sigma^*)$  states of furazan and triazole energetic molecules can be populated by nonadiabatic surface jump from the  $(\pi, \pi^*)$  or the  $(n, \pi^*)$  state. Finally, conical intersections between  $(\pi, \sigma^*)$  potential energy surfaces (PESs) and the ground PES influence the eventual fragmentation dynamics of the furazan and triazole energetic molecules. Due to structural similarity of the triazole molecule with the pyrrole molecule, a comparison of nonadiabatic dynamics of these two molecules is also presented. The N–N bond dissociation is found to be a barrierless pathway for the triazole molecule, whereas the N–H bond dissociation exhibits a barrierless pathway for the pyrrole molecule. The present work, thus, provides insights into the excited-state chemistry of furazan and triazole energetic functional groups. The same insight can also be relevant for other energetic molecules.

Published under license by AIP Publishing. <https://doi.org/10.1063/1.5088995>

## I. INTRODUCTION

Obtaining a predictive molecular understanding of the release of stored chemical energy from energetic compounds represents a major challenge for physical chemistry.<sup>1,2</sup> Energetic molecules typically release their stored chemical energy by means of different initiation events, such as laser ignition and shock waves. These initiation events can easily excite energetic species to various electronically excited states.<sup>3,4</sup> To understand the dynamics of initial fragmentation, we must know how the initial electronic excitation is eventually concentrated in chemical bonds, which can then rupture. Uncovering such mechanisms and dynamics, taking examples of furazan and triazole energetic molecules, is at the heart of the research reported in the present article.

Many interesting aspects of the decomposition of energetic molecules from the low-lying electronically excited states are already

evident from previously published results.<sup>5–7</sup> The ubiquitous role of conical intersections is evident in the de-excitation process of isolated gas phase energetic molecules. However, the importance of  $(\pi, \sigma^*)$  excited states (these electronically excited states are formed by electronic excitation from an occupied  $\pi$  orbital to an unoccupied  $\sigma^*$  orbital) in the initial step of the energy release process of different energetic molecules has not previously been evaluated or emphasized. In the present work, two nitrogen-rich energetic molecules, namely, furazan and triazole (2H-1,2,3-triazole), are selected for particular attention. These molecules are frequently used to synthesize high energy density nitrogen-rich energetic materials.<sup>8,9</sup> They give unified evidence that the electronic excitation-based initiation energy is first concentrated in certain chemical bonds of these molecules, breaking them during the initial relaxation process: a dissociative  $(\pi, \sigma^*)$  excited state controls the final mechanism and dynamics of the initial step of decomposition of these two molecules.

Before we unravel the important role of the  $(\pi, \sigma^*)$  excited states in the initial step of the energy release process of furazan and triazole energetic molecules, we briefly review the existing understanding of the role of the  $(n, \sigma^*)$  and  $(\pi, \sigma^*)$  excited states in general organic photochemistry. Over the last few years, physical and physical-organic chemistry researchers have demonstrated an increased interest (both theoretical and experimental) in the photochemistry of heteroaromatic molecules (e.g., azoles, imidazoles, azines). Excited electronic states of such molecules, termed  $(n, \sigma^*)$  and  $(\pi, \sigma^*)$  states in the recent literature, may be populated by direct photoexcitation or indirectly by nonadiabatic coupling from an optically “bright” excited state [e.g., an excited state resulting from  $(\pi, \pi^*)$  excitation]. Many examples are already documented in the literature to illustrate the photochemical importance of  $(\pi, \sigma^*)$  excited states. For example, imidazole and pyrrole, which are key chromophores in many biological molecules, exhibit electronically excited states formed via  $(\pi, \sigma^*)$  electronic excitation. Ashfold and co-workers’ recent experiments<sup>10</sup> have validated Sobolewski and co-workers’ earlier prediction<sup>11</sup> that N–H bond fission should be an important contributor to the nonradiative decay of such heteroaromatics in their  $(\pi, \sigma^*)$  states. Stolow and co-workers’ experiments<sup>12</sup> have also supported similar conclusion that a  $(\pi, \sigma^*)$  state plays a major role in the deactivation dynamics of adenine. Therefore, the important role of the  $(\pi, \sigma^*)$  excited state in the photochemistry of heteroaromatic molecules is no longer in doubt.<sup>13</sup>

The role of  $(\pi, \sigma^*)$  excited states in the initial step of decomposition of energetic molecules is still an unexplored subject. The present contribution, analyzing two families of energetic molecules (furazan and triazole), gives unambiguous and unified evidence of the important and controlling role of  $(\pi, \sigma^*)$  states in determining their explosive property at the molecular level. For the present investigation, we have involved *ab initio* electronic-structure calculations (using complete active space self-consistent field or CASSCF theory), nonadiabatic *ab initio* molecular dynamics simulations [employing the *ab initio* multiple spawning (AIMS)], and previous spectroscopic investigations of jet-cooled energetic molecules to show strong evidence of a very simple and general mechanistic picture of the dissociative, nonradiative decay of furazan and triazole-based energetic molecules.

## II. COMPUTATIONAL METHODS

The ground-state geometry of every molecule studied here was first optimized by the restricted second-order Møller–Plesset (MP2) method. These optimized geometries were then used to perform subsequent computations (including reoptimization of the ground state geometry) using the complete active space self-consistent field (CASSCF) method. The standard 6-31G(d), 6-31G(d,p), and 6-31+G(d,p) basis sets for all the atoms were used. These basis sets were selected to successfully reproduce previously observed and computed vertical excitation energies of the molecules studied here. Our previous studies show that these basis sets along with CASSCF wavefunction well reproduce electronically excited states and nonadiabatic dynamics from the  $S_1$  excited state of energetic molecules.<sup>6</sup>

For the construction of the reaction path, the coordinate-driven minimum energy path (relaxed scan) approach was adopted.

This means that for a given value of the bond length, all remaining intramolecular coordinates were optimized. These computations were performed using Molpro.<sup>14</sup> The relax scan was carried out on the  $S_1$  state with the gradient of the  $S_1$  state because, in the present work, we are interested in evolution of the  $S_1$  state only.

The shock wave or compression wave may excite the energetic species to any of their electronically excited states. These mechanical excitation processes do not necessarily follow optical excitation selection rules. This is why, in the present work, we are interested neither in photoabsorption cross section for the particular electronic excitation nor in optically bright or dark states. The focus of our present work is on the lowest-lying electronically excited  $S_1$  state of the energetic species and the ultrafast electronically nonadiabatic chemical dynamics from the respective  $S_1$  excited state.

The active space for the complete active space self-consistent field calculations for each energetic species studied here is selected keeping relevant antibonding  $\sigma^*$  orbital in mind. Minimum energy conical intersection (MECI) geometry for each energetic molecule was also optimized with state average complete active space self-consistent field (SA-CASSCF) wavefunction using the algorithm implemented in Molpro.<sup>14</sup>

Details of *ab initio* multiple spawning (AIMS) simulations can be found elsewhere.<sup>6</sup> An SA-CASSCF wavefunction is employed for the AIMS calculations because it is suitable for the computation of potential energy surfaces (PESs) particularly for the regions where two surfaces (upper and lower) come in close energy proximity (e.g., at/near conical intersections). The AIMS method,<sup>15</sup> which was developed by the Martinez group, uses the basis set approach to incorporate quantum mechanical effects for nuclear wavefunction. In this methodology, the travelling frozen (with fixed width) Gaussian basis (under frozen Gaussian approximation) is used to expand the nuclear wavefunction. In all AIMS simulations, initial positions and momenta are sampled from the Wigner distribution for the ground vibrational state (under harmonic oscillator approximation) on the ground electronic state surface.

Each AIMS simulation starts with a single trajectory basis function (TBF) on the upper electronic state. The spawning mechanism of AIMS methodology enables generation of new TBF on the lower electronic state surface, once the strength of nonadiabatic coupling increases beyond a certain threshold value (CSThresh is taken as 3.0 a.u. for all dynamics simulations performed here). This, in turn, transfers population from the upper state to the lower state. It is quite implicit that the nonadiabatic coupling is stronger near conical intersection than that near the Franck-Condon (FC) region. Therefore, spawning occurs primarily near the conical intersection region in AIMS simulation. More details of these spawning mechanisms are given in Martinez’s publications.<sup>15</sup>

In the present work, the ultrafast nonadiabatic relaxation dynamics of furazan and triazole molecules from the first singlet ( $S_1$ ) electronically excited state to the  $S_0$  ground state is studied using the AIMS module implemented in Molpro.<sup>14,15</sup> The simulation time step is set to be 20 a.u. (or 0.48 fs) for regions far away from conical intersection (regions with CSThresh <3.0 a.u.) and the same changes to 5 a.u. (or 0.12 fs) for regions near the conical intersection (regions with CSThresh >3.0 a.u., indicating strong nonadiabatic coupling).

## III. RESULTS AND DISCUSSION

## A. Initial N-O bond dissociation in furazan

Furazan (see Fig. 1 for chemical structure of furazan) is one of the novel energetic moieties which are used to synthesize nitrogen-rich energetic materials: for example, 3,3'-diamino-4,4'-azoxyfurazan (DAAF).<sup>8</sup> Decomposition of furazan following electronic excitation to the low-lying electronically excited state was experimentally studied by Bernstein and co-workers.<sup>16</sup> The following reaction scheme is evident:



Based on the experimental results and previous CASSCF calculations, one of the possible mechanisms, which ultimately renders the NO product, is via initial N-O bond dissociation, which first opens the furazan five member ring; this ring opening pathway involves a minimum energy conical intersection between the  $S_1$  and  $S_0$  states.

The most stable geometry of furazan (referred to as  $S_{0,\text{fur}}$ , see Fig. 1), optimized at the CASSCF(8,7)/6-31G(d) level of theory, exhibits a planar structure. The (8,7) active space of furazan is shown in Fig. 2(a) and is appropriately selected to include one NO antibonding  $\sigma_{\text{NO}^*}$  orbital in the active space. The role of this orbital will be explained soon. We have computed the vertical excitation energies to a few low-lying electronically excited states of the furazan molecule using the SA-CASSCF theory with the 6-31G(d) basis set. Electronic excitation characteristics associated with corresponding excitation energies are also depicted in Fig. 2(b). The SA-CASSCF(8,7)/6-31G(d) level of theory reveals that the first lowest-lying ( $n,\pi^*$ ), ( $\pi,\pi^*$ ), and ( $\pi,\sigma^*$ ) excited states of furazan possess the vertical excitation energies of 4.71, 6.16, and 10.58 eV, respectively. Furthermore, the lowest ( $\pi,\sigma^*$ ) state in the furazan system (at the Franck-Condon point or at the ground state optimized geometry,  $S_{0,\text{fur}}$ ) is classified as an electronic excitation from the ring  $\pi$  orbital to the NO  $\sigma^*$  antibonding orbital [see Fig. 2(b)]. Here, we note that the CASSCF(8,7)-calculated vertical excitation energy of the  $S_1(n,\pi^*)$  excited state of furazan shows a very

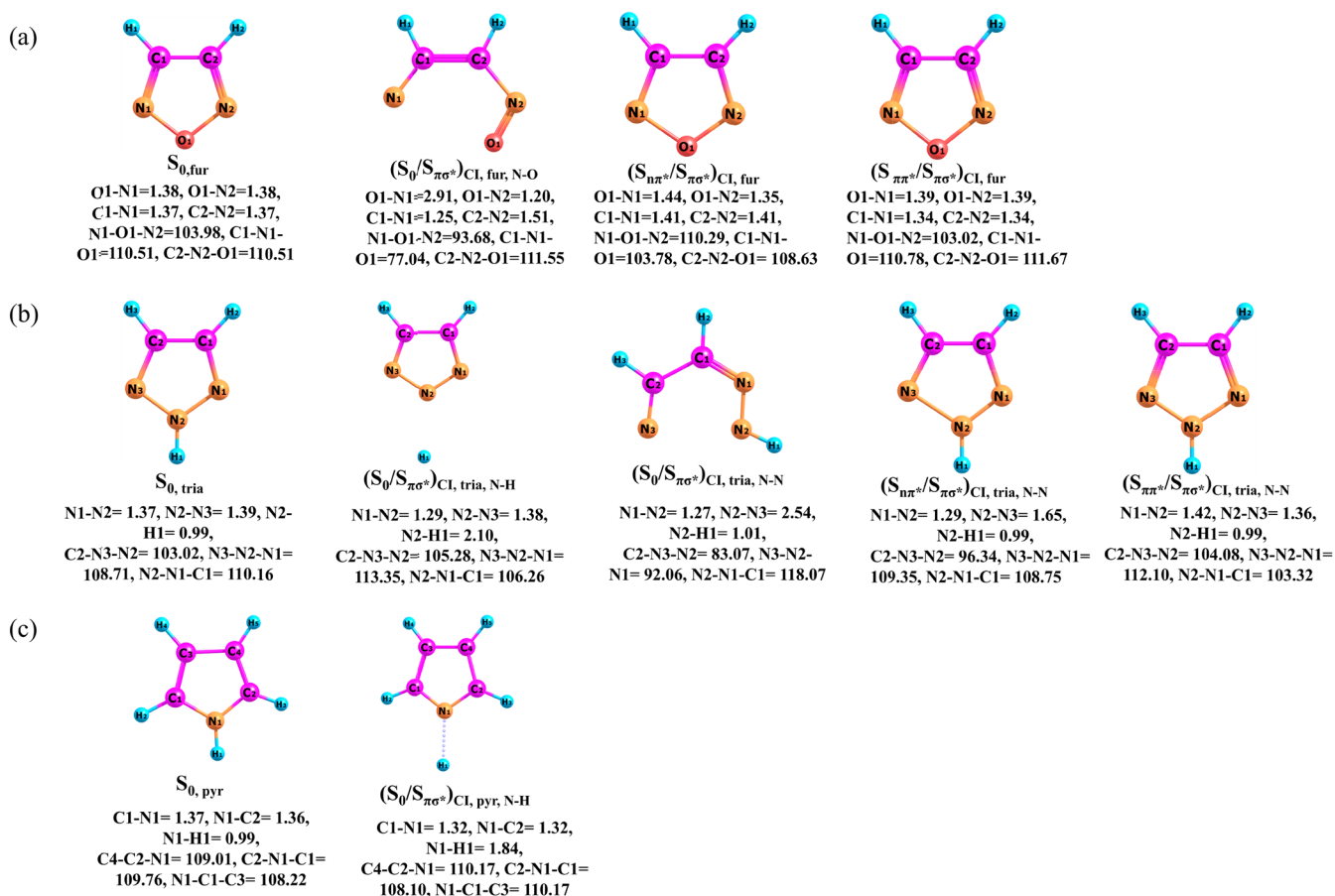


**FIG. 1.** Optimized structures of (a) furazan, (b) 2H-triazole, and (c) pyrrole. Respective ground state optimized geometries and optimized minimum energy conical intersections are shown with relevant geometrical parameters. All optimizations for the furazan molecule were performed at the CASSCF(8,7)/6-31G(d) level of theory, and the same for the 2H-triazole and pyrrole was done at the CASSCF(8,6)/6-31G(d,p) and CASSCF(8,6)/6-31+G(d,p) levels of theory, respectively.

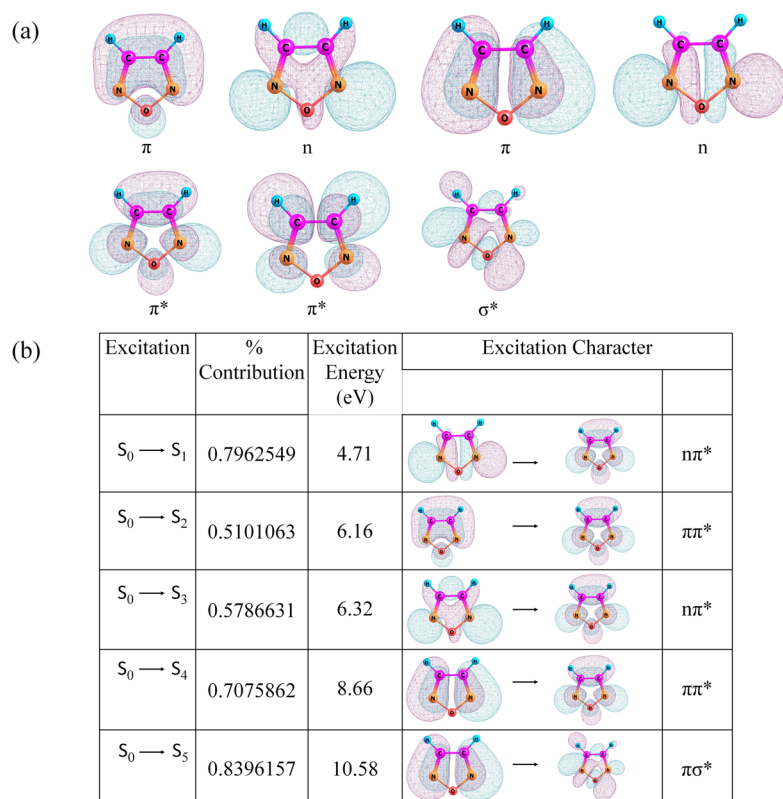


**FIG. 2.** (a) Molecular orbitals, used in the (8,7) active space of furazan, are shown. (b) Electronic excitation characters (determined from the configuration state function with the highest weight) associated with different excited state energies of furazan, as obtained at the CASSCF(8,7)/6-31G(d) level of theory, are shown.

good agreement with the previously computed CASMP2(10,7)-value of 4.70 eV.<sup>16(a)</sup>

In order to understand the initial N–O bond dissociation pathway in the spirit of involvement of a  $(\pi,\sigma^*)$  excited state, one must consider cuts through the multidimensional potential energy surfaces (PESS) of the gas phase, isolated furazan molecule, plotted against the N–O inter-nuclear distance. Figure 3(a) shows such plots: these PE curves do not change the electronic character for a certain region of the N–O inter-nuclear coordinate, and hence, that region of the curve can be identified as adiabatic (adiabatic region of the curve is represented by a single color). However, we note that the overall  $S_1$  state is diabatic because it changes character from  $(n,\pi^*)$  to  $(\pi,\sigma^*)$  (note the red to green color change for the  $S_1$  state). Figure 3(b) can easily help one identify the excitation character at different positions of the scan. To maintain clarity in the presentation of Fig. 3(a), only the lowest energy  $(n,\pi^*)$ ,  $(\pi,\pi^*)$ , and  $(\pi,\sigma^*)$  states are shown along with the ground state. The PE curves shown in Fig. 3(a) feature minimum-energy reaction-path profiles: these profiles are constructed by optimizing the values of all coordinates except for the given value of the reaction coordinate (more technically they are called relaxed scan profiles) and are obtained at the CASSCF(8,7)/6-31G(d) level of theory.

Figure 3(a) reveals that both the  $(n,\pi^*)$  and  $(\pi,\pi^*)$  states are bound, but the  $(\pi,\sigma^*)$  state is repulsive (dissociative) with respect to the N–O stretch coordinate. The dissociative nature (shape) of the  $(\pi,\sigma^*)$  PE profile in the furazan system originates from the

fact that the  $\sigma^*$  antibonding character provides a strong driving force for the N–O bond dissociation in the respective  $(\pi,\sigma^*)$  state. Figure 3(a) also indicates that the  $(\pi,\sigma^*)$  potential curve eventually correlates with the ground state and thus should exhibit a conical intersection with the  $S_0$  PES. In fact, one minimum energy conical intersection (MECI) point for furazan is located through the CASSCF(8,7)/6-31G(d) level of theory: the corresponding optimized geometry is given in Fig. 1 [see  $(S_0/S_{\pi,\sigma^*})_{\text{Cl,fur,NO}}$  geometry]. The structure of furazan at this MECI clearly exhibits a very elongated N–O bond with respect to the ground state optimized geometry. Here, we note that the speculation of existence of other conical intersections, such as the one between the  $(n,\pi^*)$  and  $(\pi,\sigma^*)$  states and the one between the  $(\pi,\pi^*)$  and  $(\pi,\sigma^*)$  states, made by relaxed scan was further confirmed by locating the respective minimum energy conical intersections (see Fig. 1 for the respective optimized geometries). The relative energies of the minimum energy  $(S_{n\pi^*}/S_{\pi\sigma^*})_{\text{Cl,fur}}$ ,  $(S_{\pi\pi^*}/S_{\pi\sigma^*})_{\text{Cl,fur}}$ , and  $(S_0/S_{\pi\sigma^*})_{\text{Cl,fur,N-O}}$  conical intersections with respect to the energy of the ground state optimized geometry are found to be 4.65, 6.08, and 0.99 eV, respectively.

Therefore, the key point for the nonadiabatic reaction of furazan, as revealed from the above computational results, is the predissociative nature of the lowest-lying excited  $(n,\pi^*)$  and  $(\pi,\pi^*)$  excited states induced by the repulsive  $(\pi,\sigma^*)$  state. Furazan shows that a  $(\pi,\pi^*)$ – $(\pi,\sigma^*)$  curve crossing and a  $(n,\pi^*)$ – $(\pi,\sigma^*)$  curve crossing occur at an intermediate N–O distance [see Fig. 3(a)]. Therefore, one can easily speculate from Fig. 3(a) that radiationless

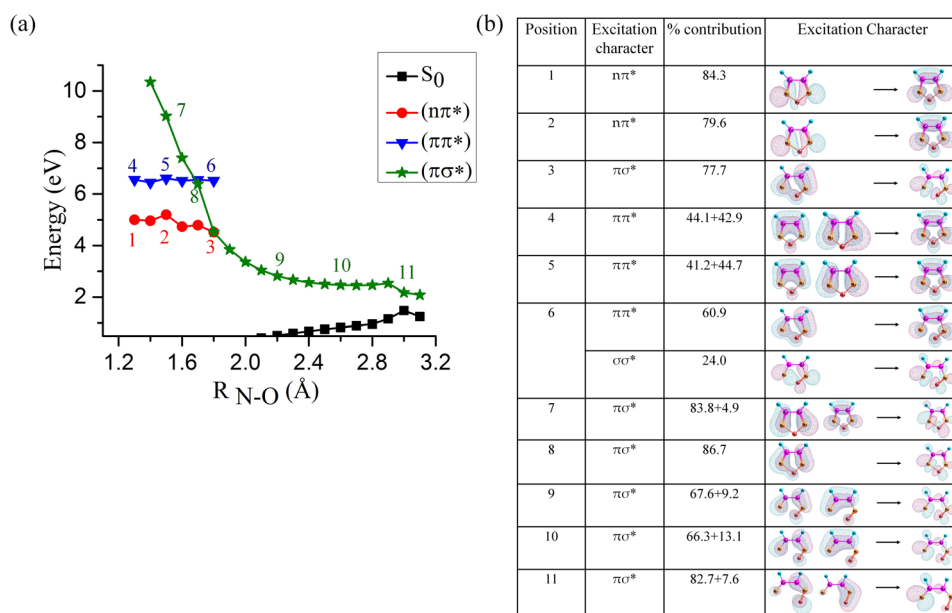


**FIG. 3.** (a) The PE profiles for the ground and the lowest-lying excited ( $n,\pi^*$ ), ( $\pi,\pi^*$ ), and ( $\pi,\sigma^*$ ) states of furazan plotted against the N–O stretch coordinate,  $R_{N-O}$ . These profiles are obtained at the CASSCF(8,7)/6-31G(d) level of theory. (b) Electronic excitation characters associated with CSF's percent contributions at different positions of the scan are depicted.

transfer to the ( $\pi,\sigma^*$ ) state after excitation to either of the ( $n,\pi^*$ ) and ( $\pi,\pi^*$ ) states may constitute efficient nonadiabatic decay routes for the furazan moiety. This decay route accompanies the initial N–O bond dissociation (through the ring opening mechanism) and eventually transfers population to the ground electronic state.

The qualitative topographical features of the PE curves resulting from the crossing of a repulsive ( $\pi,\sigma^*$ ) state with bound ( $n,\pi^*$ ) and ( $\pi,\pi^*$ ) states are directly manifested in the ultrafast relaxation process of this molecule, as evident in Figs. 4(a) and 4(b). Figure 4(a) depicts the change in average population of the furazan molecule on the  $S_1$  excited state as a function of the simulation time (femtoseconds), as revealed by the AIMS simulations performed at the SA-CASSCF(8,7)/6-31G(d) level of theory. We find that the quenching of the  $S_1$  excited state population to the ground electronic state for the furazan molecule occurs in approximately 133 fs. The nonadiabatic decay occurs through the N–O bond dissociation (via a ring opening mechanism). See Fig. 4(b) for closer inspection of the variation of the relevant N–O bond distance of the furazan molecule as a function of simulation time. We find that the average N–O bond elongates as the molecule approaches the ( $S_0/S_{\pi,\sigma^*}$ )<sub>CI,fur,NO</sub> conical intersection: this supports the ring opening mechanism. The AIMS-predicted ring opening mechanism was previously predicted as one of the decomposition mechanisms of the furazan molecule following electronic excitation to its lowest-lying electronically excited state;<sup>16</sup> however, the time scale for the ring opening mechanism was not computed earlier. Furthermore, the role of the dissociative ( $\pi,\sigma^*$ ) state was not previously explored.

## B. Initial N–N bond dissociation of 2H-1,2,3-triazole

The recent literature unambiguously corroborates the fact that the key role in the nonradiative decay of pyrrole (see Fig. 1 for

the chemical structure) is played by the excited singlet state of ( $\pi,\sigma^*$ ) character.<sup>10</sup> Here, the ( $\pi,\sigma^*$ ) excited state features electronic excitation to an antibonding  $\sigma^*$  N–H orbital. 2H-triazole (see Fig. 1 for chemical structure) is structurally very similar to

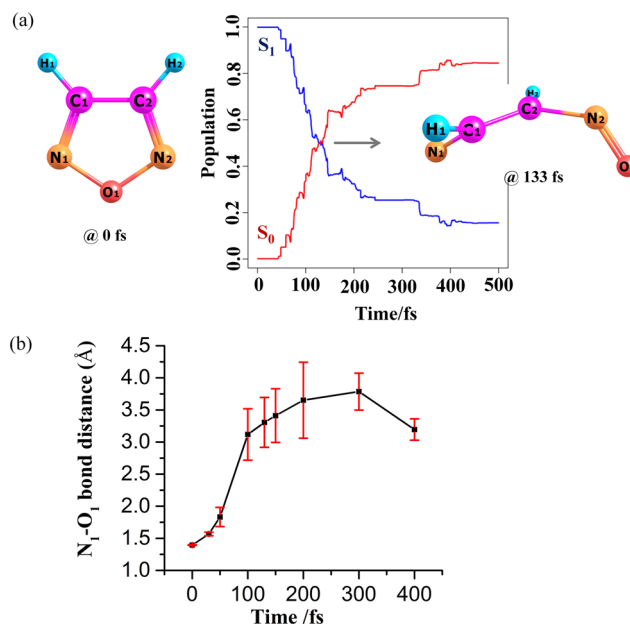
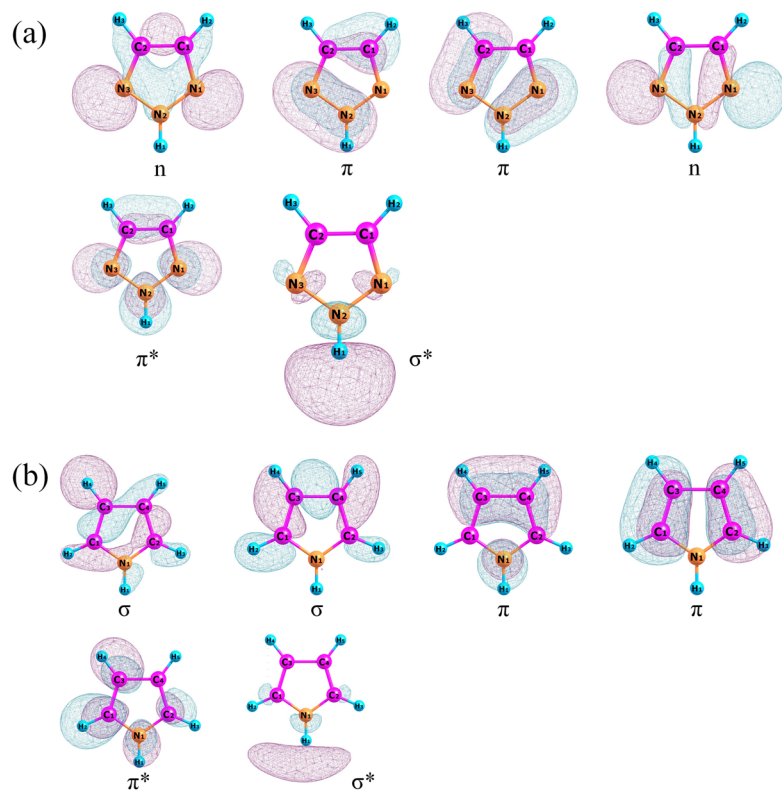


**FIG. 4.** (a) Plots of average population of the first excited state ( $S_1$ , blue) and of the ground state ( $S_0$ , red) of furazan as a function of simulation time, as revealed by the AIMS simulation using the SA-CASSCF(8,7)/6-31G(d) wave function. (b) Plots of average  $N_1-O_2$  bond distance (in Å) of furazan as a function of simulation time. All plots represent an average of 17 independent AIMS simulations. The error bar represents the standard deviation of the mean.

pyrrole and has often been employed as an energetic functional group which is introduced to candidate compounds to obtain better energetic materials.<sup>9</sup> Structural and eventual electronic similarity of 2H-triazole and pyrrole serve as motivation to explore the decomposition mechanisms and dynamics of 2H-triazole from a  $(\pi, \sigma^*)$  perspective.

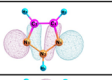
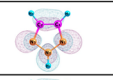
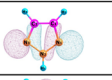
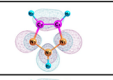
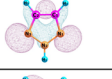
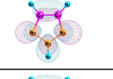
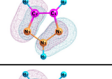
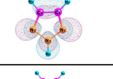
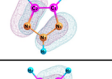
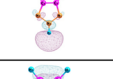
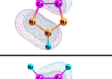
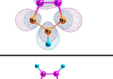
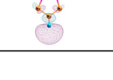
The most stable geometries of 2H-triazole and pyrrole (referred to as  $S_{0,\text{tria}}$  and  $S_{0,\text{pyr}}$ , respectively), optimized, respectively, at the CASSCF(8,6)/6-31G(d,p) and CASSCF(8,6)/6-31+G(d,p) levels of theory, are illustrated in Fig. 1. We have used a diffuse basis function to include the  $\sigma^*$  orbital in the active space of pyrrole. Both molecules exhibit planar structure. The (8,6) active space for both molecules is depicted in Fig. 5. Note that the (8,6) active space includes the NH antibonding  $\sigma^*$  orbital for both molecules. The vertical excitation energies and electronic excitation character of both molecules are compared and contrasted in Fig. 6. Quite interestingly, the  $(\pi, \sigma^*)$  state, which is characterized by electronic excitation to the antibonding NH  $\sigma^*$  state, stays lower in energy than the  $(n, \pi^*)$  and  $(\pi, \pi^*)$  states in pyrrole. 2H-triazole, on the other hand, exhibits quite the opposite trend in the relative alignment of the vertical excited states. The  $(\pi, \sigma^*)$  state is the lowest-lying electronically excited state of pyrrole, whereas the lowest-lying electronically excited state of 2H-triazole has an  $(n, \pi^*)$  character. Therefore, based on the vertical electronic excitation characteristics of the two molecules, the excited state chemistry of these two molecules may differ significantly.

Figure 7(a) shows that PE curves obtained from the cuts of the multidimensional potential energy surfaces (PESs) of the gas phase isolated pyrrole molecule plotted against the  $N_1-H_1$  distance. The PE curves were obtained from the relaxed scan at the CASSCF(8,6)/6-31+G(d,p) level of theory. It is quite evident that the  $(\pi, \pi^*)$  state of pyrrole is not a dissociative state, whereas both lowest-lying  $(\pi, \sigma^*)$  states are dissociative. The  $(\pi, \sigma^*)$  state of pyrrole stays below the  $(\pi, \pi^*)$  state not only at the Franck-Condon (FC) point but also for the entire N-H nuclear coordinate. Therefore, the electronic excitation-induced chemistry of the  $S_1$  excited state of pyrrole should be determined by the dynamics of the  $(\pi, \sigma^*)$  surface and its conical intersection with the ground state. In fact, the conical intersection between  $(\pi, \sigma^*)$  and the ground state is found to be responsible for the ultrafast deactivation of pyrrole via an H-atom detachment pathway.<sup>10</sup> The same is also evident through the present AIMS simulations, as shown in Figs. 7(b) and 7(c). Quenching of the  $S_1$  excited state population to the ground electronic state for pyrrole occurs in approximately 22 fs. Recently, the nonadiabatic dynamics of pyrrole from the  $(\pi, \sigma^*)$  state have been studied using time-resolved photoelectron spectroscopy (TRPES) and wavepacket propagations using the multiconfigurational time-dependent Hartree (MCTDH) method.<sup>17</sup> The TRPES spectra suggest a decay time constant of 12 fs. This decay time constant is in very good agreement with the AIMS-predicted lifetime of the  $(\pi, \sigma^*)$  state of pyrrole. Finally, AIMS simulation results exhibit elongation of the average N-H bond as a function of the simulation time [see Fig. 7(c)]. Involvement of

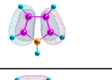
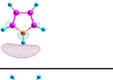
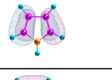
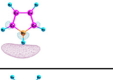
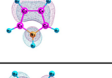
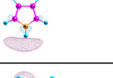
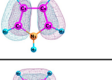
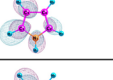
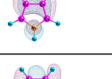
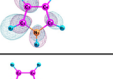
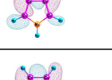
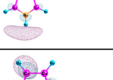
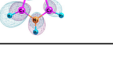


**FIG. 5.** Molecular orbitals, used in the (8,6) active space of (a) 2H-triazole and (b) pyrrole, are shown. These orbitals are obtained at the CASSCF(8,6)/6-31G(d,p) and the CASSCF(8,6)/6-31+G(d,p) level of theory, respectively, for 2H-triazole and pyrrole.

(a)

Excitation	Contribution	Excitation Energy (eV)	Excitation Character			
				→		
$S_0 \rightarrow S_1$	0.6528231	5.28		→		$n\pi^*$
$S_0 \rightarrow S_2$	0.5973245	7.24		→		$n\pi^*$
$S_0 \rightarrow S_3$	0.4338295	8.56		→		$\pi\pi^*$
$S_0 \rightarrow S_4$	0.6042495	8.66		→		$\pi\sigma^*$
$S_0 \rightarrow S_5$	0.4687617	9.52		→		$\pi\pi^*$
$S_0 \rightarrow S_6$	0.5909833	10.46		→		$\pi\sigma^*$

(b)

Excitation	Contribution	Excitation Energy (eV)	Excitation Character			
				→		
$S_0 \rightarrow S_1$	0.945031	4.97		→		$\pi\sigma^*$
$S_0 \rightarrow S_2$	0.943841	5.95		→		$\pi\sigma^*$
$S_0 \rightarrow S_3$	0.657524	7.98		→		$\pi\pi^*$
$S_0 \rightarrow S_4$	0.636143	8.84		→		$\pi\pi^*$
$S_0 \rightarrow S_5$	0.910509	10.35		→		$\sigma\sigma^*$
$S_0 \rightarrow S_6$	0.969979	10.63		→		$\sigma\pi^*$

**FIG. 6.** Electronic excitation characters (determined from the configuration state function with the highest weight) associated with different excited state energies of (a) 2H-triazole and (b) pyrrole, as obtained at the CASSCF(8,6)/6-31G(d,p) and the CASSCF(8,6)/6-31+G(d,p) level of theory, respectively.

an H-atom detachment mechanism [see Fig. 7(c)] is suggested with the help of the AIMS simulations, in agreement with the previous report.<sup>17</sup>

Figure 8(a) shows that the PE curves obtained from the cuts of the multidimensional potential energy surfaces (PESs) of the gas phase isolated 2H-triazole molecule plotted against the N–N distance (which opens the ring). Excitation characters at different positions of the N–N scan can be identified from Fig. 8(b). On the other hand, Fig. 8(c) depicts the cuts of the multidimensional potential energy surfaces (PESs) of the same molecule plotted against the N–H inter-nuclear distance. Excitation characters at different positions of the N–H scan are depicted in Fig. 8(d). All the scans were performed at the CASSCF(8,6)/6-31G(d,p) level of theory.

It is clearly evident in Fig. 8 that the nature of the  $(\pi, \sigma^*)$  state in Figs. 8(a) and 8(c) is different. The  $(\pi, \sigma^*)$  state shown in Fig. 8(a)

corresponds to the promotion of electron from the ring  $\pi$  orbital to the N–N  $\sigma^*$  orbital. On the other hand, the  $(\pi, \sigma^*)$  state shown in Fig. 8(c) corresponds to the promotion of electron from the ring  $\pi$  orbital to the N–H  $\sigma^*$  orbital. Furthermore, with respect to the FC point of the  $S_1$  excited state [which exhibits an  $(n, \pi^*)$  character], N–N bond dissociation is a barrierless pathway for 2H-triazole, whereas the N–H bond dissociation pathway exhibits a barrier height of 1.36 eV [this barrier represents the energy difference between the  $(n, \pi^*)$ – $(\pi, \sigma^*)$  crossing point and the FC point of the  $S_1(n, \pi^*)$  state]. We note that the energetic location of the crossing between the  $(\pi, \sigma_{\text{NH}}^*)$  state and the lowest-lying  $(n, \pi^*)$  state is significantly different from that between the  $(\pi, \sigma_{\text{NN}}^*)$  state and the lowest-lying  $(n, \pi^*)$  state. With regard to the respective Franck-Condon points on the  $S_1$  surface, a barrier is evident for the  $(n, \pi^*)$ – $(\pi, \sigma_{\text{NH}}^*)$  curve crossing at an intermediate N–H bond distance, but almost no barrier

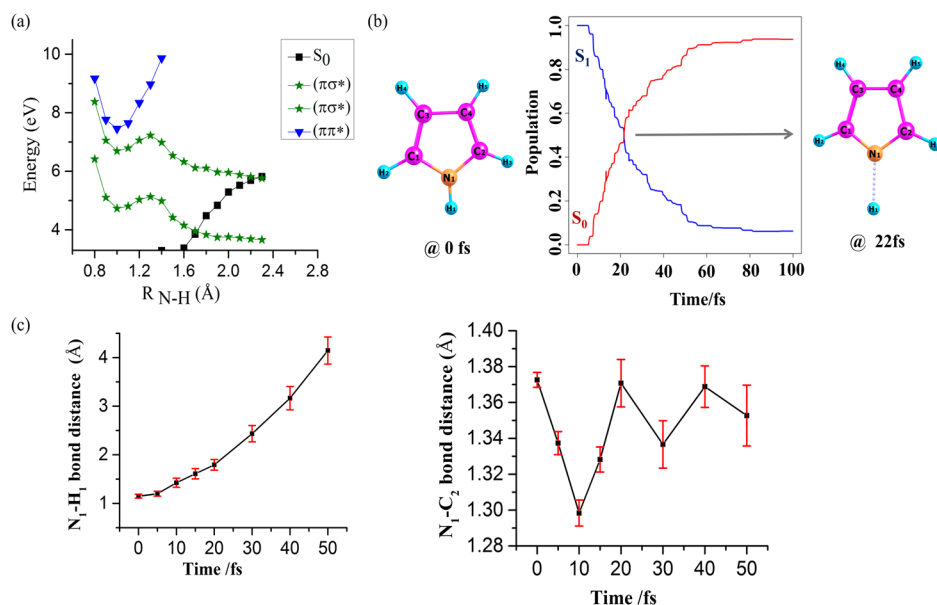


**FIG. 7.** (a) The PE profiles for the ground and the lowest-lying excited ( $\pi,\sigma^*$ ) and ( $\pi,\pi^*$ ) states of pyrrole plotted against the N–H stretch coordinate. These profiles are obtained at the CASSCF(8,6)/6-31+G(d,p) level of theory. (b) Plots of average population of the first excited state ( $S_1$ , blue) and of the ground state ( $S_0$ , red) of pyrrole as a function of simulation time, revealed by the AIMS simulation using the SA-CASSCF(8,6)/6-31+G(d,p) wave function. (c) Plots of average  $N_1$ – $H_1$  (left figure) and  $N_1$ – $C_2$  (right figure) bond distances (in Å) as a function of simulation time. All plots in (b) and (c) represent an average of 22 independent AIMS simulations. The error bar represents the standard deviation of the mean. The  $N_1$ – $C_2$  bond length exhibits a sense of oscillation; however, we believe that more sampling should smear out this apparent oscillation because the change in bond length is found to be in the range of 0.07–0.08 Å.

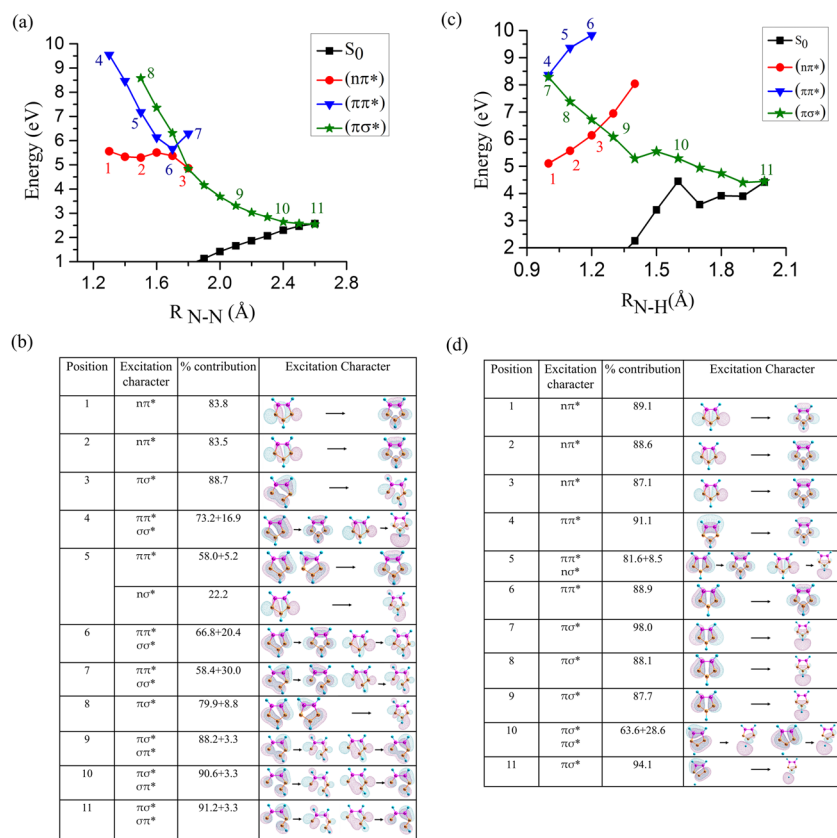


**FIG. 8.** (a) The PE profiles for the ground and the lowest-lying excited ( $n,\pi^*$ ), ( $\pi,\pi^*$ ) and ( $\pi,\sigma^*$ ) states of 2H-triazole plotted against the N–N stretch coordinate. (b) Electronic excitation characters associated with CSF's percent contributions at different positions of the N–N scan for 2H-triazole. (c) The PE profiles for the ground and the lowest-lying excited ( $n,\pi^*$ ), ( $\pi,\pi^*$ ), and ( $\pi,\sigma^*$ ) states of 2H-triazole plotted against the N–H stretch coordinate. (d) Electronic excitation characters associated with CSF's percent contributions at different positions of the N–H scan for 2H-triazole. All relaxed scans were performed at the CASSCF(8,6)/6-31G(d,p) level of theory.

Position	Excitation character	% contribution	Excitation Character
1	$n\pi^*$	83.8	
2	$n\pi^*$	83.5	
3	$\pi\sigma^*$	88.7	
4	$\pi\pi^*$ $\sigma\sigma^*$	73.2+16.9	
5	$\pi\pi^*$	58.0+5.2	
	$n\sigma^*$	22.2	
6	$\pi\pi^*$ $\sigma\sigma^*$	66.8+20.4	
7	$\pi\pi^*$ $\sigma\sigma^*$	58.4+30.0	
8	$\pi\sigma^*$	79.9+8.8	
9	$\pi\sigma^*$ $\sigma\pi^*$	88.2+3.3	
10	$\pi\sigma^*$ $\sigma\pi^*$	90.6+3.3	
11	$\pi\sigma^*$ $\sigma\pi^*$	91.2+3.3	

Position	Excitation character	% contribution	Excitation Character
1	$n\pi^*$	89.1	
2	$n\pi^*$	88.6	
3	$n\pi^*$	87.1	
4	$\pi\pi^*$	91.1	
5	$\pi\pi^*$ $\pi\sigma^*$	81.6+8.5	
6	$\pi\pi^*$	88.9	
7	$\pi\sigma^*$	98.0	
8	$\pi\sigma^*$	88.1	
9	$\pi\sigma^*$	87.7	
10	$\pi\sigma^*$ $\pi\sigma^*$	63.6+28.6	
11	$\pi\sigma^*$	94.1	

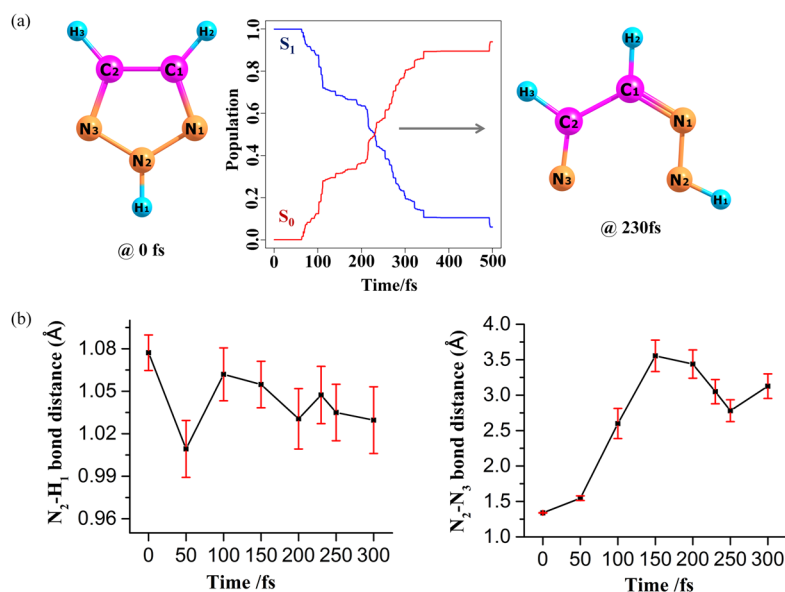


**FIG. 9.** (a) Plots of average population of the first excited state ( $S_1$ , blue) and of the ground state ( $S_0$ , red) of 2H-triazole as a function of simulation time, as revealed by the AIMS simulation using the SA-CASSCF(8,6)/6-31G(d) wave function. (b) Plots of average  $N_2-H_1$  (left figure) and  $N_2-N_3$  (right figure) bond distances (in Å) as a function of simulation time. All plots represent an average of 30 independent AIMS simulations. The error bar represents the standard deviation of the mean. The  $N_2-H_1$  bond length exhibits a sense of oscillation; however, we believe that more sampling should smear out this apparent oscillation because the change in bond length is found to be in the range of 0.07–0.08 Å.

is evident for the similar  $(n,\pi^*)-(\pi,\sigma_{NN}^*)$  curve crossing at an intermediate N–N bond distance. Therefore, chemical dynamics of 2H-triazole following electronic excitation to the  $S_1(n,\pi^*)$  excited state is expected to be controlled by the crossing between the  $(\pi,\sigma_{NN}^*)$  state and the ground state surface.

The above qualitative argument is evident from Fig. 9, which depicts AIMS simulation results for 2H-triazole. Figure 9(a) depicts the change in average population of the 2H-triazole molecule on the respective  $S_0$  ground and the  $S_1$  excited states as a function of the simulation time. We find that the quenching of the  $S_1$  excited state population to the ground electronic state for this molecule occurs in approximately 230 fs. Furthermore, Figs. 9(a) and 9(b) depict that only the N–N bond dissociation channel is active in the deactivation process of the 2H-triazole molecule. The H-atom detachment channel is inactive in the deactivation process for 2H-triazole. Therefore, although 2H-triazole is structurally similar to pyrrole, their decomposition mechanisms and dynamics from the lowest-lying electronically excited state differ significantly due to a difference in relative energy alignment of the  $(\pi,\sigma^*)$  state with respect to the  $(\pi,\pi^*)$  or the  $(n,\pi^*)$  states.

#### IV. GENERAL DISCUSSION AND CONCLUSIONS

Our present work unambiguously suggests that predissociation plays a ubiquitous role in the initial step of energy release processes for energetic molecules of the kind presented in this article. Herzberg, through his seminal studies, classified predissociation processes into types I and II: type-I refers to predissociation via electronic coupling and type-II refers to predissociation via vibrational coupling to the reaction coordinate.<sup>18</sup> Molecules in the type-I case jump over different electronic surfaces by electronic coupling, whereas a single adiabatic potential energy surface is involved in type-II predissociation. Vibrational coupling to the reaction coordinate via intramolecular vibrational redistribution (IVR) is mainly

responsible for type-II predissociation. The nature of predissociation (explored here taking examples of furan and triazole) which ultimately predestines the fate of the energetic molecules following electronic excitation is of the type-I kind. This is why chemical dynamics of energetic molecules will ultimately be controlled by the complexity of potential energy surfaces near surface-crossing regions (conical intersections).<sup>16(b)</sup>

The present study emphasizes that the  $(\pi,\sigma^*)$  excited electronic states play a pivotal role in the initial steps of decomposition of energetic molecules of the kind studied here. The potential energy surfaces of the  $(\pi,\sigma^*)$  states are dissociative along the respective  $\sigma$  bond stretch coordinate. The repulsive character of the  $(\pi,\sigma^*)$  states originates from the facts that it is primarily localized on a single  $\sigma$  bond and that it is antibonding with regard to the respective  $\sigma$  bond. Surface crossing (conical intersection) of the dissociative  $(\pi,\sigma^*)$  state with the lowest-lying bound  $(n,\pi^*)$  and  $(\pi,\pi^*)$  states of energetic molecules predissociates these low-lying excited states. Finally, the  $(\pi,\sigma^*)$  PE surfaces exhibit a conical intersection with the electronic ground-state PE surface: this intersection provides the mechanism for ultrafast deactivation to the ground state via decomposition. Thus, energetic molecules find an efficient way to concentrate initiation energy (gained via electronic excitation) in a particular  $\sigma$  bond through the  $(\pi,\sigma^*)$  state: this ultimately controls the initial step of decomposition of energetic molecules. Therefore, the conical intersection between the  $(\pi,\sigma^*)$  PE surface and the ground state surface must play a ubiquitous role in the initial step of decomposition of energetic molecules of the kind studied here. Further study is necessary to generalize the conclusion for all energetic molecules.

Due to the structural similarity of the triazole molecule with the pyrrole molecule, a comparison of nonadiabatic dynamics of these two molecules is explored in the present work. With respect to the FC point of the  $S_1(n,\pi^*)$  excited state of the triazole and pyrrole molecules, the N–N dissociation is found to be a barrierless pathway

for the triazole molecule, whereas the N–H bond dissociation pathway exhibits a barrierless pathway for the pyrrole molecule. These two molecules not only exhibit different decomposition mechanisms but also show different relative alignments of the  $(\pi, \sigma^*)$  state with respect to the lowest-lying  $(n, \pi^*)$  state. The high-lying dissociative  $(\pi, \sigma^*)$  state makes the lowest-lying  $(n, \pi^*)$  state predissociative in the triazole molecule: this is a feature which is also observed for the furazan molecule but is not observed for pyrrole.

Conical intersections play an essential role in many nonadiabatic processes, including several basic biological processes, in particular, vision and photosynthesis. For the last several years, taking several examples of energetic molecules, the important role of conical intersections in the decomposition of energetic molecules has been emphasized.<sup>5–7</sup> Energetic molecules store a large amount of chemical energy, and this chemical energy is released when they decompose. From a fundamental point of view, one important question remains open: how is the initiation energy concentrated in the chemical bonds of an energetic molecule to result in decomposition. Or, in other words, what does control the initial step of the energy release process of energetic molecules? We argue that via predissociation of the lowest-lying  $(\pi, \pi^*)$  and  $(n, \pi^*)$  states and a conical intersection with the ground state, the  $(\pi, \sigma^*)$  state triggers a dissociative ultrafast deactivation process, which might be essential for the energy release behavior of energetic molecules. We have tested this argument with the help of furazan and triazole examples.

## ACKNOWLEDGMENTS

This work was supported by IISc Space Technology Cell (IISc-STC, India) under Contract No. STC/P-333. We thank Dr. Sai G. Ramesh (IPC, IISc) for maintaining departmental computational cluster facility.

## REFERENCES

- 1 R. W. Shaw, T. B. Brill, and D. L. Thompson, “Overviews of recent research on energetic materials,” *Adv. Ser. Phys. Chem.* **16**, 532 (2005).
- 2 G. F. Adams and R. W. Shaw, “Chemical reactions in energetic materials,” *Annu. Rev. Phys. Chem.* **43**, 311 (1992).
- 3 E. R. Bernstein, “Role of excited electronic states in the decomposition of energetic materials,” *Overview Recent Res. Energ. Mater.* **16**, 000161 (2005); H.-S. Im and E. R. Bernstein, “On the initial steps in the decomposition of energetic materials from excited electronic states,” *J. Chem. Phys.* **113**, 7911 (2000).
- 4 F. E. Williams, “Electronic states of solid explosives and their probable role in detonations,” *Adv. Chem. Phys.* **21**, 289 (1971). J. Sharma, B. C. Beard, and M. Chaykovsky, “Correlation of impact sensitivity with electronic levels and structure of molecules,” *J. Phys. Chem.* **95**, 1209 (1991). J. Gilman, “Chemical reactions at detonation fronts in solids,” *Philos. Mag. B* **71**, 1057 (1995). M. M. Kukulja, B. P. Aduiev, E. D. Aluker, V. I. Krasheninina, A. G. Krechetov, and A. Y. Mitrofanov, “Role of electronic excitations in explosive decomposition of solids,” *J. Appl. Phys.* **89**, 4156 (2001).
- 5 A. Bhattacharya, Y. Guo, and E. R. Bernstein, “Experimental and theoretical exploration of the initial steps in the decomposition of a model nitramine energetic material: Dimethylnitramine,” *J. Phys. Chem. A* **113**, 000811–823 (2009). A. Bhattacharya, Y. Guo, and E. R. Bernstein, “Unimolecular decomposition of tetrazine-N-oxide based high nitrogen content energetic materials from excited electronic states,” *J. Chem. Phys.* **131**, 194304 (2009). B. Yuan and E. R. Bernstein, “Initial mechanisms for the unimolecular decomposition of electronically excited bisfuroxan based energetic materials,” *J. Chem. Phys.* **146**, 014301 (2017).
- 6 B. Yuan and E. R. Bernstein, “Initial mechanisms for the unimolecular decomposition of electronically excited nitrogen-rich energetic salts with tetrazole rings:  $(\text{NH}_4)_2\text{BT}$  and TAGzT,” *J. Chem. Phys.* **145**, 064306 (2016). B. Yuan, Z. Yu, and E. R. Bernstein, “Initial mechanisms for the decomposition of electronically excited energetic materials: 1,5’-BT, 5,5’-BT, and AzTT,” *J. Chem. Phys.* **142**, 124315 (2015). B. Yuan, Z. Yu, and E. R. Bernstein, “Initial decomposition mechanism for the energy release from electronically excited energetic materials: FOX-7 (1,1-diamino-2,2-dinitroethene,  $\text{C}_2\text{H}_4\text{N}_4\text{O}_4$ ),” *J. Chem. Phys.* **140**, 074708 (2014). Z. Yu and E. R. Bernstein, “On the decomposition mechanisms of new imidazole-based energetic materials,” *J. Phys. Chem. A*, **117**, 1756–1764 (2013). Z. Yu and E. R. Bernstein, “Experimental and theoretical studies of the decomposition of new imidazole based energetic materials: Model systems,” *J. Chem. Phys.* **137**, 114303 (2012).
- 7 A. Bera, J. Ghosh, and A. Bhattacharya, “*ab Initio* multiple spawning dynamics study of dimethylnitramine and dimethylnitramine-Fe complex to model their ultrafast nonadiabatic chemistry,” *J. Chem. Phys.* **147**, 044308 (2017). J. Ghosh, S. Banerjee, and A. Bhattacharya, “AIMS simulation study of ultrafast electronically nonadiabatic chemistry of methyl azide and UV-VIS spectroscopic study of azido-based energetic plasticizer bis(1,3-diazido prop-2-yl)malonate,” *Chem. Phys.* **494**, 78–89 (2017). J. Ghosh, H. Gajapathy, A. Konar, and G. M. Narasimhaiah, “A. BhattacharyaSub-500 fs electronically nonadiabatic chemical dynamics of energetic molecules from the  $S_1$  excited state: *ab initio* multiple spawning study,” *J. Chem. Phys.* **147**, 204302 (2017).
- 8 J. Soto, J. F. Arenas, J. C. Otero, and D. Peláez, “Effect of an  $(S_1/S_0)$  conical intersection on the chemistry of nitramide in its ground state. A comparative CASPT2 study of the nitro-nitrite isomerization reactions in nitramide and nitromethane,” *J. Phys. Chem. A* **110**, 8221–8226 (2006). J. F. Arenas, J. C. Otero, D. Peláez, and J. Soto, “CASPT2 study of the decomposition of nitrosomethane and its tautomerization reactions in the ground and low-lying excited states,” *J. Org. Chem.* **71**, 983–991 (2006). H. Wu, Y. Song, G. Yu, Y. Wang, C. Wang, and Y. Yang, “Tracking the photodissociation dynamics of liquid nitromethane at 266 nm by femtosecond time-resolved broadband transient grating spectroscopy,” *Chem. Phys. Lett.* **652**, 152–156 (2016).
- 9 D. E. Chavez, M. A. Hiskey, and R. D. Gilardi, “3,3’-Azobis(6-amino-1,2,4,5-tetrazine): A novel high-nitrogen energetic material,” *Angew. Chem., Int. Ed.* **39**, 1791 (2000). D. E. Chavez, L. Hill, M. Hiskey, and S. Kinkead, “Preparation and explosive properties of azo- and azoxy-furazans,” *J. Energ. Mater.* **18**, 219 (2000). D. E. Chavez and M. A. Hiskey, “High nitrogen pyrotechnic compositions,” *J. Pyrotech.* **7**, 11 (1998).
- 10 H. Gao and J. M. Shreeve, “Azole-based energetic salts,” *Chem. Rev.* **111**, 7377–7436 (2011). T. Klapötke, *Chemistry of High-Energy Materials*, 2nd ed. (de Gruyter, Berlin, 2012).
- 11 M. N. R. Ashfold, B. Cronin, A. L. Devine, R. N. Dixon, and M. G. D. Nix, “The role of  $\pi\sigma^*$  excited states in the photodissociation of heteroaromatic molecules” *Science* **312**, 1637 (2006).
- 12 A. L. Sobolewski, W. Domcke, C. Dedonder-Lardeux, and C. Jouvet, “Excited-state hydrogen detachment and hydrogen transfer driven by repulsive  $^1\pi\sigma^*$  states: A new paradigm for nonradiative decay in aromatic biomolecules,” *Phys. Chem. Chem. Phys.* **4**, 1093 (2002).
- 13 H. Satzger, D. Townsend, M. Z. Zgierski, S. Patchkovskii, S. Ullrich, and A. Stolow, “Primary processes underlying the photostability of isolated DNA bases: Adenine,” *Proc. Natl. Acad. Sci. U. S. A.* **103**, 10196 (2006).
- 14 M. N. R. Ashfold, G. A. King, D. Murdock, M. G. D. Nix, T. A. A. Oliver, and A. G. Sage, “ $\pi\sigma^*$  excited states in molecular photochemistry,” *Phys. Chem. Chem. Phys.* **12**, 1218–1238 (2010).
- 15 H.-J. Werner, P. J. Knowles, G. Knizia, F. R. Manby, M. Schütz, P. Celani, T. Korona, R. Lindh, A. Mitrushenkov, G. Rauhut, K. R. Shamasundar, T. B. Adler, R. D. Amos, A. Bernhardsson, A. Berning, D. L. Cooper, M. J. O. Deegan, A. J. Dobson, F. Eckert, E. Goll, C. Hampel, A. Hesselmann, G. Hetzer, T. Hrenar, G. Jansen, C. Köppl, Y. Liu, A. W. Lloyd, R. A. Mata, A. J. May, S. J. McNicholas, W. Meyer, M. E. Mura, A. Nicklass, D. P. O’Neill, P. Palmieri, D. Peng, K. Pflüger, R. Pitzer, M. Reiher, T. Shiozaki, H. Stoll, A. J. Stone, R. Tarroni, T. Thorsteinsson, and M. Wang, *MOLPRO*, version 2012.1.
- 16 B. G. Levine, J. D. Coe, A. M. Virshup, and T. J. Martinez, “Implementation of *Ab initio* multiple spawning in the Molpro quantum chemistry package,” *Chem. Phys.* **347**, 3 (2008). M. Ben-Nun and T. J. Martínez, “*ab Initio* quantum molecular dynamics,” *Adv. Chem. Phys.* **121**, 439 (2002).

<sup>16</sup>(a) Y. Q. Guo, A. Bhattacharya, and E. R. Bernstein, "Excited electronic state decomposition of furazan based energetic materials: 3,3-diamino-4,4-azoxyfurazan and its model systems, diaminofurazan and furazan," *J. Chem. Phys.* **128**, 034303 (2008). (b) A. Bhattacharya, Y. Guo, and E. R. Bernstein, "Nonadiabatic reaction of energetic molecules," *Acc. Chem. Res.* **43**, 1476–1485 (2010).

<sup>17</sup>G. Wu, S. P. Neville, O. Schalk, T. Sekikawa, M. N. R. Ashfold, G. A. Worth, and A. Stolow, "Excited state non-adiabatic dynamics of pyrrole: A time-resolved photoelectron spectroscopy and quantum dynamics study," *J. Chem. Phys.* **142**, 074302 (2015).

<sup>18</sup>R. Schinke, *Photodissociation Dynamics* (Cambridge University Press, 2009).